ELSEVIER

Engineering Analysis with Boundary Elements 30 (2006) 88–99

ENGINEERING ANALYSIS *with* BOUNDARY ELEMENTS

www.elsevier.com/locate/enganabound

Two-dimensional time-harmonic BEM for cracked anisotropic solids

F. García-Sánchez [a], A. Sáez [b,*], J. Domínguez [b]

[a] *Departamento de Ingeniería Civil, E.T.S. de Ingenieros Industriales, Universidad de Málaga, Campus de El Ejido s/n, 29013 Málaga, Spain*
[b] *Departamento de Mecánica de Medios Continuos, Escuela Superior de Ingenieros, Universidad de Sevilla, Camino de los Descubrimientos s/n, 41092 Sevilla, Spain*

Received 14 January 2005; received in revised form 23 August 2005; accepted 21 September 2005
Available online 28 November 2005

Abstract

A mixed time-harmonic boundary element procedure for the analysis of two-dimensional dynamic problems in cracked solids of general anisotropy is presented. To the author's knowledge, no previous BE approach for time-harmonic two-dimensional crack problems in anisotropic solids exists. In the present work, the fundamental solution is split into the static singular part plus dynamic regular terms. Hypersingular integrals associated to the singular part in the traction boundary integral equation are transformed, by means of a simple change of variable, into regular ones plus very simple singular integrals with known analytical solution. Subsequently, only regular (frequency dependent) terms have to be added to the regularized static fundamental solution in order to solve the dynamic problem. The generality of this procedure permits the use of general straight or curved quadratic boundary elements. In particular, discontinuous quarter-point elements are used to represent the crack-tip behavior. Stress intensity factors are accurately computed from the nodal crack opening displacements at discontinuous quarter-point elements. The efficiency and robustness of the present time-harmonic BEM are verified numerically by several test examples. Results are also obtained for more complex configurations, not previously studied in the literature. They include curved crack geometry.

Keywords: Boundary element method; Anisotropic solids; Fracture mechanics; Dynamics; Curved crack.

1. Introduction

Two of the engineering fields for which boundary elements (BE) have reached a higher degree of development are wave propagation (dynamics of continua) and fracture mechanics. Topics like dynamic soil–structure interaction or wave scattering by discontinuities of any type, have received particular attention within the first of these two fields. Two outstanding papers by Beskos [10,11] and the book of Domínguez [20] contain a review of most of the work in this area until 1996. In the second field, fracture mechanics, many problems of different type have been analyzed using BE or other integral equation approaches. A comprehensive review of the work until 1997 can be found in the paper by Aliabadi [6]. Particularly important in this area are formulations based on the traction boundary integral equation (BIE); i.e. hypersingular and mixed (or dual) formulations, where the requirement of multi-domain techniques is avoided by use of the traction BIE over the crack boundaries. The first formulations of this type were presented by Ioakimidis in 1983 [27] and Hong and Chen in 1988 [26]. A general review of the use of traction BIE for crack problems can be found in [6], and an analysis of the regularization requirements associated to it in [50]. As it can be seen in those review papers, a large majority of the fracture mechanics BE studies are restricted to isotropic solids.

Most work dealing with BE solutions of crack problems in anisotropic solids have been carried out in the last 10 years, although some pioneering papers, like those written by Cruse and Swedlow [15], Snyder and Cruse [45], Doblaré et al. [19], Tan and Gao [49], and Sollero and Aliabadi [46,47], were published prior to 1995. The procedures developed in those seminal works contained limitations related to the type of material or the crack geometry, or required the use of multi-domain techniques.

Sollero and Aliabadi [48] first presented a general mixed BE formulation for cracked 2D anisotropic solids in 1995. A similar formulation, with a different stress intensity factor (SIF) computation technique, was presented by Pan and Amadei [35] and extended by Pan [36] and Pan et al. [37] to cracks in semi-infinite 2D anisotropic domains. A hypersingular integral equation approach for cracks in two dissimilar elastic half-planes was also presented by Ang and Park [7].

* Corresponding author. Tel.: +34 954487293; fax: +34 954487295.
E-mail addresses: andres@us.es (A. Sáez), fgsanchez@uma.es (F. García-Sánchez), jose@us.es (J. Domínguez).

0955-7997/$ - see front matter © 2005 Elsevier Ltd. All rights reserved.
doi:10.1016/j.enganabound.2005.09.005

More recently, hypersingular and mixed BE formulations have been extended to crack problems in 3D anisotropic solids [8,34,38,40,51]. These papers are related to static anisotropic crack problems. There is also a small number of publications dedicated to BE formulations for dynamic problems in anisotropic solids. Most difficulties in those formulations are related to the complexity of the available fundamental solutions, which are known in terms of integrals over infinite or finite domains [21,53,54]. Three-dimensional dynamic problems have been analyzed by Kögl and Gaul [31], Niu and Dravinski [33] and Sáez and Domínguez [41,42].

Ariza and Domínguez [9] have presented a formulation for the analysis of time-harmonic crack problems in three-dimensional transversely isotropic solids, based on the traction BIE and quarter-point boundary elements. They used the fundamental solution obtained by Wang and Achenbach [53,54].

BE formulations for wave scattering in 2D anisotropic solids were presented by Kobayashi et al. [30] in 1986 and by Wang et al. [55] in 1996. More recently, Ahmad et al. [1] have used a BE procedure based on Green's functions written in terms of infinite integrals to study dynamic soil–structure interaction problems in 2D anisotropic media. Denda et al. [17] have proposed a frequency domain formulation for 2D solids of general anisotropy. They have applied this general formulation to eigenvalue analysis of simple geometry 2D domains.

The study of 2D crack problems in anisotropic solids using BE is restricted to a very small number of papers published in the last few years. Zhang [56] has presented a hypersingular time-domain traction BE approach for transient dynamic analysis of cracked orthotropic infinite solids. He uses a convolution quadrature formula in combination with a Laplace domain Green's function. Hirose et al. [25] carried out a comparative study of that procedure and a time domain formulation, which makes use of the time-domain fundamental solution [54]. They use the formulation presented by Wang et al. [55] and a Galerkin discretization. These authors computed dynamic SIF for a straight crack in an infinite solid subjected to an impact load. Alburquerque et al. [2–5] have recently presented a Dual Reciprocity formulation for general anisotropic 2D dynamic crack problems.

In the present paper, a frequency domain mixed boundary element approach for crack problems in anisotropic media is presented. To the authors' knowledge, no previous BE formulation for time-harmonic two-dimensional crack problems in anisotropic solids exists. The formulation proposed is general and can be used for unbounded and finite domain crack problems. It is based on the use of the traction integral representation at nodes of a single crack surface and the displacement integral representation at nodes over the external boundaries when the solid is finite. The time-harmonic fundamental solution presented by Wang and Achenbach [53,54] is used. It is decomposed into a singular part (static) with strongly singular and hypersingular first and second derivatives, respectively, and a frequency dependent regular part. The proposed approach is applied to domains including single or multiple cracks with straight and curved geometries. Strongly singular and hypersingular integrals appearing in the formulation are transformed into regular ones by a simple analytical transformation valid for elements with any arbitrary geometry. A BE formulation for cracks in anisotropic solids under static loading, based on the same principles, has been recently presented by the authors [23].

During the review process of the present paper, an article by Dineva et al. [18], where these authors present a BE approach for dynamic cracked anisotropic materials based on the classical non-hypersingular BE formulation, has been published.

2. Mixed BEM for fracture applications in anisotropic elastodynamics

The dual or mixed formulation of the BEM makes use of both displacement and traction boundary integral equations (BIE).

2.1. Displacement BIE and fundamental solution

The 2D displacement integral representation for a point ξ in an elastic anisotropic domain Ω with boundary Γ can be written for time-harmonic loading conditions as

$$c_{ij}(\xi)u_j(\xi,\omega)+\int_\Gamma p^*_{ij}(\boldsymbol{x},\xi,\omega)u_j(\boldsymbol{x},\omega)\mathrm{d}\Gamma(\boldsymbol{x}) = \int_\Gamma u^*_{ij}(\boldsymbol{x},\xi,\omega)p_j(\boldsymbol{x},\omega)\mathrm{d}\Gamma(\boldsymbol{x}) \quad (1)$$

where $i,j=1,2$; ω is the angular frequency of excitation; ξ is the collocation point and $\boldsymbol{x}$ is the observation point; u^*_{ij} and p^*_{ij} are the elastodynamic fundamental solution displacements and tractions, respectively; and $c_{ij}(\xi)$is the so-called free term that results from the Cauchy principal value (CPV) integration of the strongly singular p^*_{ij} kernels.

The fundamental solution displacements in 2D anisotropic elastic media under time-harmonic loading have been obtained by Wang and Achenbach [53,54] based on the Radon transform. Their solution is given in the form of a contour integral over a unit circle

$$u^*_{ij}(\boldsymbol{x},\xi,\omega)=\frac{1}{8\pi^2}\int_{|\boldsymbol{\eta}|=1}\sum_{m=1}^{2}\frac{V_{im}(\boldsymbol{\eta})V_{jm}(\boldsymbol{\eta})}{\rho c_m^2(\boldsymbol{\eta})}\Psi(k_m|\boldsymbol{\eta}\cdot(\boldsymbol{x}-\xi)|)\mathrm{d}S(\boldsymbol{\eta}) \quad (2)$$

where $\boldsymbol{\eta}=(\eta_1,\eta_2)$ is a unit vector describing the position on the unit circle and $V_{im}(\boldsymbol{\eta})$are the eigenvectors of the Christoffel matrix defined as

$$\Gamma_{ij}(\boldsymbol{\eta})=C_{pijq}\eta_p\eta_q \quad (3)$$

where C_{pijq} are the elastic constants of the anisotropic material. The eigenvalues of $\Gamma_{ij}(\boldsymbol{\eta})$ are $\lambda_m(\boldsymbol{\eta})=\rho c_m^2(\boldsymbol{\eta})$. That is

$$\Gamma_{ij}(\boldsymbol{\eta})V_{jm}(\boldsymbol{\eta})=\lambda_m(\boldsymbol{\eta})V_{im}(\boldsymbol{\eta}) \ \ (\text{no sum on } m) \quad (4)$$

c_m thus being the phase velocities and $k_m = \omega/c_m$ the wave numbers. In Eq. (2)

$$\Psi(s) = i\pi \exp(is) - 2[\cos(s)\mathrm{Ci}(s) + \sin(s)\mathrm{Si}(s)] \tag{5}$$

where $\mathrm{Ci}(s)$ and $\mathrm{Si}(s)$ stand for the cosine and sine integrals

$$\mathrm{Ci}(s) = -\int_s^\infty \frac{\cos t}{t}\mathrm{d}t; \quad \mathrm{Si}(s) = -\int_s^\infty \frac{\sin t}{t}\mathrm{d}t \tag{6}$$

The Green's functions in Eq. (2) may be decomposed into the sum of singular plus regular parts

$$u^*_{ij}(\boldsymbol{x},\boldsymbol{\xi},\omega) = u^{*\mathrm{S}}_{ij}(\boldsymbol{x},\boldsymbol{\xi}) + u^{*\mathrm{R}}_{ij}(\boldsymbol{x},\boldsymbol{\xi},\omega) \tag{7}$$

The singular part corresponds to the anisotropic Green's functions for elastostatics

$$u^{*\mathrm{S}}_{ij}(\boldsymbol{x},\boldsymbol{\xi}) = \frac{-1}{4\pi^2} \int_{|\boldsymbol{\eta}|=1} \sum_{m=1}^{2} \frac{V_{im}(\boldsymbol{\eta})V_{jm}(\boldsymbol{\eta})}{\rho c_m^2(\boldsymbol{\eta})} \log|\boldsymbol{\eta}\cdot(\boldsymbol{x}-\boldsymbol{\xi})|\mathrm{d}S(\boldsymbol{\eta}) \tag{8}$$

whilst the regular part is frequency dependent

$$u^{*\mathrm{R}}_{ij}(\boldsymbol{x},\boldsymbol{\xi},\omega) = \frac{1}{8\pi^2} \int_{|\boldsymbol{\eta}|=1} \sum_{m=1}^{2} \frac{V_{im}(\boldsymbol{\eta})V_{jm}(\boldsymbol{\eta})}{\rho c_m^2(\boldsymbol{\eta})} \Psi^{\mathrm{R}}(k_m, |\boldsymbol{\eta}\cdot(\boldsymbol{x}-\boldsymbol{\xi})|)\mathrm{d}S(\boldsymbol{\eta}) \tag{9}$$

where

$$\Psi^{\mathrm{R}}(k_m, |\boldsymbol{\eta}\cdot(\boldsymbol{x}-\boldsymbol{\xi})|) = \Psi(k_m|\boldsymbol{\eta}\cdot(\boldsymbol{x}-\boldsymbol{\xi})|) + 2\log|\boldsymbol{\eta}\cdot(\boldsymbol{x}-\boldsymbol{\xi})| \tag{10}$$

is a regular continuous function.

There exist a classic explicit elastostatic fundamental solution for anisotropic solids obtained by Eshelby et al. [22] using the complex variable solution approach

$$u^{*\mathrm{S}}_{ij}(\mathrm{x},\xi) = -\frac{1}{\pi}\mathrm{Re}\left\{\sum_{m=1}^{2} A_{jm}H_{mi}\ln(z^x_m - z^\xi_m)\right\} \tag{11}$$

where z^ξ and z^x are, respectively, the source and the observation point defined on the complex plane as

$$z^\xi_m = \xi_1 + \mu_m\xi_2; \qquad z^x_m = x_1 + \mu_m x_2; \quad m = 1,2 \tag{12}$$

μ_m being the roots of the characteristic equation of the anisotropic material

$$|C_{1ij1} + (C_{1ij2} + C_{2ij1})\mu_m + C_{2ij2}\mu_m^2| = 0 \tag{13}$$

where C_{mijn} are the elastic constants of the anisotropic material.

The roots of (13) are either complex or purely imaginary and always occur in conjugate pairs [22]. For each of these characteristic roots μ_m, the columns of the $\boldsymbol{A}$ matrix are obtained from

$$[C_{1ij1} + (C_{1ij2} + C_{2ij1})\mu_m + C_{2ij2}\mu_m^2]A_{jm} = 0 \quad \text{(no sum on } m\text{)} \tag{14}$$

and matrix $\boldsymbol{H}$ is obtained from

$$\boldsymbol{H} = \boldsymbol{A}^{-1}(\boldsymbol{B}^{-1} + \bar{\boldsymbol{B}}^{-1})^{-1} \quad \text{with } \boldsymbol{B} = i\boldsymbol{A}\boldsymbol{L}^{-1} \tag{15}$$

where the components of the $\boldsymbol{L}$ matrix are given by

$$L_{im} = \sum_{j=1}^{2}[C_{2ij1} + C_{2ij2}\mu_m]A_{jm} = -\frac{1}{\mu_m}\sum_{j=1}^{2}[C_{1ij1} + C_{1ij2}\mu_m]A_{jm} \quad \text{(no sum on } m\text{)} \tag{16}$$

The elastostatic Green's functions defined in Eqs. (8) and (11) only differ by the constant terms $\varkappa_{ij}$ (see Ref. [17] for details)

$$\varkappa_{ij} = \frac{1}{\pi}\mathrm{Re}\left\{\sum_{m=1}^{2} A_{jm}H_{mi}\ln(\mathrm{i} - \mu_m)\right\}; \quad (\mathrm{i} = \sqrt{-1}) \tag{17}$$

These constants are inessential for the elastostatic BEM formulation [23], but they are required for the time-harmonic fundamental solution displacements to maintain the quiescent field ahead of the wavefront produced by the line force.

For the sake of efficiency, the static fundamental solution due to Eshelby (11) will be used as singular part of the dynamic solution instead of (8). The dynamic solution will be completed by adding the frequency dependent regular part given by Eq. (9). The computer time required for evaluation of (11) is significantly smaller than that needed for evaluation of the static singular part of the time-harmonic fundamental solution. The obtained results present the same accuracy in both cases.

The corresponding fundamental solution tractions are obtained for the singular part by derivation of the displacements in Eq. (11) and substitution into Hooke's law to yield

$$p^{*\mathrm{S}}_{ij}(\boldsymbol{x},\boldsymbol{\xi}) = -\frac{C_{rjln}}{\pi}\mathrm{Re}\left\{\sum_{m=1}^{2} A_{lm}H_{mi}\frac{z^x_{m,n}}{z^x_m - z^\xi_m}\right\}n_r \tag{18}$$

where $z^x_{m,n}$ follows from (12)

$$z^x_{m,n} = \frac{\partial z^x_m}{\partial x_n} = \delta_{1n} + \mu_m\delta_{2n}; \quad m,n = 1,2 \tag{19}$$

Using Eq. (16), the elastostatic tractions (18) can be rewritten as

$$p^{*\mathrm{S}}_{ij}(\boldsymbol{x},\boldsymbol{\xi}) = \frac{1}{\pi}\mathrm{Re}\left\{\sum_{m=1}^{2} L_{jm}H_{mi}\frac{\mu_m n_1 - n_2}{z^x_m - z^\xi_m}\right\} \tag{20}$$

Similarly, the regular part of the fundamental solution tractions are obtained from (9) as

$$p^{*\mathrm{R}}_{ij}(\boldsymbol{x},\boldsymbol{\xi},\omega) = \frac{1}{8\pi^2} \int_{|\boldsymbol{\eta}|=1} \sum_{m=1}^{2} \frac{V_{im}(\boldsymbol{\eta})V_{rm}(\boldsymbol{\eta})}{\rho c_m^2(\boldsymbol{\eta})} \bar{\Gamma}_{jr}k_m\psi(k_m|\boldsymbol{\eta}\cdot(\boldsymbol{x}-\boldsymbol{\xi})|)\mathrm{sign}[\boldsymbol{\eta}\cdot(\boldsymbol{x}-\boldsymbol{\xi})]\mathrm{d}S(\boldsymbol{\eta}) \tag{21}$$

where

$$\bar{\Gamma}_{jr} = C_{mjrl}\eta_m\eta_l \tag{22}$$

and

$$\psi(k_m|\boldsymbol{\eta}\cdot(\boldsymbol{x}-\boldsymbol{\xi})|) = \frac{\partial \Psi^{\mathrm{R}}(k_m, |\boldsymbol{\eta}\cdot(\boldsymbol{x}-\boldsymbol{\xi})|)}{\partial x_l} \tag{23}$$

so that

$$\psi(s) = -\pi \exp(is) - 2[\cos(s)\mathrm{Si}(s) - \sin(s)\mathrm{Ci}(s)] \tag{24}$$

2.2. Traction BIE

The 2D traction integral representation for a source point $\boldsymbol{\xi}$ with unit normal $\boldsymbol{N}$ is obtained by differentiation of the displacement BIE (1) with respect to ξ_k and the subsequent application of Hooke's law, to yield

$$c_{ij}(\boldsymbol{\xi})p_j(\boldsymbol{\xi},\omega) + N_r \int_\Gamma s^*_{rij}(\boldsymbol{x},\boldsymbol{\xi},\omega)u_j(\boldsymbol{x},\omega)\mathrm{d}\Gamma(\boldsymbol{x}) = N_r \int_\Gamma d^*_{rij}(\boldsymbol{x},\boldsymbol{\xi},\omega)p_j(\boldsymbol{x},\omega)\mathrm{d}\Gamma(\boldsymbol{x}) \tag{25}$$

where s^*_{ijk} and d^*_{ijk} are therefore obtained by differentiation of p^*_{ij} and u^*_{ij}, respectively, with the following expressions

$$d^*_{ijk} = -C_{ijml}u^*_{mk,l} \tag{26}$$

$$s^*_{ijk} = -C_{ijml}p^*_{mk,l} \tag{27}$$

where, l indicates $\partial/\partial x_l$ and $\partial/\partial\xi_l = -\partial/\partial x_l$ has been considered.

Derivatives of the fundamental solution displacements at the collocation point are evaluated from

$$\frac{\partial u^{*\mathrm{S}}_{ij}(\boldsymbol{x},\boldsymbol{\xi})}{\partial \xi_l} = -\frac{1}{\pi}\mathrm{Re}\left\{\sum_{m=1}^{2} A_{jm}H_{mi}\frac{z^{\xi}_{m,l}}{z^x_m - z^{\xi}_m}\right\} \tag{28}$$

for the singular part and

$$\frac{\partial u^{*\mathrm{R}}_{ij}(\boldsymbol{x},\boldsymbol{\xi},\omega)}{\partial \xi_l} = \frac{1}{8\pi^2}\int_{|\boldsymbol{\eta}|=1}\sum_{m=1}^{2}\frac{V_{im}(\boldsymbol{\eta})V_{jm}(\boldsymbol{\eta})}{\rho c^2_m(\boldsymbol{\eta})}k_m\eta_l \psi(k_m|\boldsymbol{\eta}\cdot(\boldsymbol{x}-\boldsymbol{\xi})|)\mathrm{sign}[\boldsymbol{\eta}\cdot(\boldsymbol{x}-\boldsymbol{\xi})]\mathrm{d}S(\boldsymbol{\eta}) \tag{29}$$

for the regular part.

Similarly, derivatives of the fundamental solution tractions at the collocation point are obtained as

$$\frac{\partial p^{*\mathrm{S}}_{ij}(\boldsymbol{x},\boldsymbol{\xi})}{\partial \xi_l} = -\frac{1}{\pi}\mathrm{Re}\left\{\sum_{m=1}^{2} L_{jm}H_{mi}\frac{\mu_m n_1 - n_2}{(z^x_m - z^{\xi}_m)^2}z^{\xi}_{m,l}\right\} \tag{30}$$

for the singular part of the solution and as

$$\frac{\partial p^{*\mathrm{R}}_{ij,l}(\boldsymbol{x},\boldsymbol{\xi},\omega)}{\partial \xi_l} = -\frac{1}{8\pi^2}\int_{|\boldsymbol{\eta}|=1}\sum_{m=1}^{2}\frac{V_{im}(\boldsymbol{\eta})V_{rm}(\boldsymbol{\eta})}{\rho c^2_m(\boldsymbol{\eta})}\bar{\Gamma}_{jr}k^2_m\eta_l \Psi(k_m|\boldsymbol{\eta}\cdot(\boldsymbol{x}-\boldsymbol{\xi})|)\mathrm{sign}[\boldsymbol{\eta}\cdot(\boldsymbol{x}-\boldsymbol{\xi})]\mathrm{d}S(\boldsymbol{\eta}) \tag{31}$$

for the regular part, where $\Psi(s)$ is defined in Eq. (5).

2.3. Mixed BEM for fracture mechanics

Let Γ_C be the uncracked boundary and Γ_+ and Γ_- the two crack surfaces boundaries. In the dual BEM [5], the displacement BIE (1) is applied on Γ_C and one of the crack faces, say Γ_-, whilst the traction BIE (25) is applied on the opposite crack face Γ_+. However, if the tractions on the two crack surfaces are equal and opposite ($\Delta p_k = p^+_k + p^-_k = 0$) it is enough to consider the displacement BIE applied on Γ_C

$$c_{ij}u_j + \int_{\Gamma_C} p^*_{ij}u_j\,\mathrm{d}\Gamma + \int_{\Gamma_+} p^*_{ij}\Delta u_j\,\mathrm{d}\Gamma = \int_{\Gamma_C} u^*_{ij}p_j\,\mathrm{d}\Gamma \tag{32}$$

and the traction BIE applied on one side of the crack faces Γ_+

$$p_i + N_r\int_{\Gamma_C} s^*_{rij}u_j\,\mathrm{d}\Gamma + N_r\int_{\Gamma_+} s^*_{rij}\Delta u_j\,\mathrm{d}\Gamma = N_r\int_{\Gamma_C} d^*_{rij}p_j\,\mathrm{d}\Gamma \tag{33}$$

to define a complete set of equations to obtain the tractions and displacements on the boundary and the crack opening displacements (CODs) $\Delta u_k = u^+_k - u^-_k$ along the crack. There is a strong singularity of order $0\,[1/(z^x_m - z^{\xi}_m)]$ in the displacement BIE (32) and a hypersingularity of order $0\,[1/(z^x_m - z^{\xi}_m)^2]$ in the traction BIE (33). Therefore, these integrals have to be computed in the sense of a Cauchy principal value (CPV) and a Hadamard finite part (HFP), respectively. Note that in Eq. (33), the free term has been set to 1 to account for the additional singularity arising from the coincidence of the two crack surfaces.

The discretization approach follows García et al. [23]. The C^1 continuity condition of the displacements at collocation points in the traction BIE is fulfilled by using discontinuous quadratic elements to mesh the crack. To reproduce the displacements behavior near the crack-tip, simple straight-line discontinuous quadratic elements with the mid-node located at one quarter of the element length are used. Standard continuous quadratic elements are considered for the rest of the boundary, except for the case when there is an intersection between a crack and an external boundary. In such a case, a semi-discontinuous element is used on the outer boundary to avoid a common node at the intersection.

2.4. Dynamic stress intensity factors computation

Consider a polar coordinate system r–θ centered at the crack-tip and such that $\theta = \pm\pi$ are the crack surfaces. Then, the shear (Δu_1) and normal (Δu_2) components of the COD near the crack-tip may be written in terms of the mode I (K_{I}) and mode II (K_{II}) stress intensity factors (SIFs) as [43]

$$\begin{pmatrix}\Delta u_1\\ \Delta u_2\end{pmatrix} = \sqrt{\frac{8r}{\pi}}\begin{pmatrix}D_{11} & D_{12}\\ D_{21} & D_{22}\end{pmatrix}\begin{pmatrix}K_{\mathrm{I}}(\omega)\\ K_{\mathrm{II}}(\omega)\end{pmatrix} + \text{higher order terms} \tag{34}$$

where

$$D_{11} = \mathrm{Im}\left(\frac{\mu_2 A_{11} - \mu_1 A_{12}}{\mu_1 - \mu_2}\right);$$
$$D_{12} = \mathrm{Im}\left(\frac{A_{11} - A_{12}}{\mu_1 - \mu_2}\right); \quad D_{21} = \mathrm{Im}\left(\frac{\mu_2 A_{21} - \mu_1 A_{22}}{\mu_1 - \mu_2}\right); \quad (35)$$
$$D_{22} = \mathrm{Im}\left(\frac{A_{21} - A_{22}}{\mu_1 - \mu_2}\right)$$

the matrix $\boldsymbol{A}$ being the one defined in (14).

In order to capture this square-root behavior of the COD, straight-line quarter-point quadratic crack-tip elements are used, as previously presented in a mixed formulation context for elastostatic isotropic and anisotropic solids by Sáez et al. [39] and García et al. [23], respectively.

The quarter-point element technique was developed for the classical BE formulation by Cruse and Wilson [16], Blandford et al. [12], Smith and Mason [44] and Martínez and Domínguez [32] among others.

Within this element the relationship between the distance to the crack front r and the boundary element natural coordinate ζ is given by

$$\zeta = 2\sqrt{\frac{r}{L}} - 1 \quad (36)$$

L being the quarter-point element length.

In the present work, the collocation nodes NC1, NC2 and NC3 for the quarter-point element are located at $\zeta_1 = -3/4$, $\zeta_2 = 0$ and $\zeta_3 = +3/4$, respectively, as done for elastostatics [23,39]. In such case, the distance r from the collocation nodes of the quarter-point element to the crack-tip follows from Eq. (36)

$$r_1 = \frac{L}{64} \text{ for NC1}; \qquad r_2 = \frac{L}{4} \text{ for NC2}$$
$$r_3 = \frac{49L}{64} \text{ for NC3} \quad (37)$$

Particularizing Eq. (34) for the collocation node NC1 ($r = L/64$) the following one-point formula for the direct evaluation of the SIF may be obtained

$$\begin{Bmatrix} K_{\mathrm{II}} \\ K_{\mathrm{I}} \end{Bmatrix} = 2\sqrt{2\pi/L}(\mathrm{Re}\{\boldsymbol{B}\})^{-1} \begin{Bmatrix} \Delta u_1^{\mathrm{NC1}} \\ \Delta u_2^{\mathrm{NC1}} \end{Bmatrix} \quad (38)$$

Several other approaches to evaluate the SIF directly from the computed nodal values may be considered, as described by Sáez et al. [39] for the isotropic case. However, the procedure presented in Eq. (38) is more accurate and less mesh-dependent than any other, since the SIF is calculated from the COD at a collocation point extremely close to the crack front, where the $\sqrt{r}$ behavior of the COD is highly dominant.

3. Numerical implementation

The decomposition of the fundamental solution into singular static plus regular dynamic terms separates the integrals in the singular displacement BIE and the hypersingular traction BIE into their elastostatic counterparts plus regular integrals which are numerically evaluated. In this manner, the static problem is dealt with by following the approach developed by García et al. [23], and then the regular (frequency dependent) terms are added to solve the dynamic problem.

The regularization procedure presented by García et al. [23] for the static singular and hypersingular parts of the kernels is based on a simple change of variables that transforms all the strongly singular and hypersingular integrals, prior to any numerical evaluation, into regular integrals plus very simple singular integrals with known analytical solution. A detailed explanation of this procedure may be found in García et al. [23].

The regular dynamic part of the fundamental solution is given in terms of line integrals over a unit circumference. This fact leads to a double numerical integration: first over the unit circumference and second over the boundary element. In the case of the s^*_{rij} kernels, though, the derivative of the regular part of the fundamental solution tractions (31) show a weak singularity that is accounted for by means of a logarithmic quadrature.

Alternatively, in Wang et al. [55] and Denda et al. [17], straight elements are considered for the displacement BIE, and the order of integration is exchanged provided that the dynamic terms are regular. Then, the integration over the boundary element is done analytically, leaving only the line integral over the unit circumference for numerical evaluation. In Ref. [17], a detailed error analysis for the numerical computation of the dynamic part is carried out to propose a reliable integration scheme that is used in this paper.

4. Numerical applications

Application of the proposed formulation and numerical scheme is illustrated next. Several examples relative to solids of different material properties with one or more, straight or curved cracks, are considered. The accuracy and robustness of the approach is tested by solving some problems whose solution has been previously obtained by other authors using different procedures. Kinked and curved crack problems, which had never been studied before for anisotropic materials, are also analyzed.

Infinite and finite domain problems have been studied. In the first type of problems, the excitation consist of impinging waves of the two possible kinds existing in infinite domains; i.e. P and S-waves. Finite domain problems are considered under the effects of dynamic forces applied at the boundaries.

Stress-free boundary conditions on crack surfaces has been posed in all considered examples.

It is worth to mention that the crack is considered to remain open during oscillation. This fact makes sense in two situations: one is when the time-harmonic load is applied superimposed to static loading conditions such that the overall crack-tip opening displacement remains positive all the time; the other situation is when time-harmonic results are used for frequency domain analysis of transient dynamic problems. In this case, superimposition is a linear mathematical operation

and results are valid as long as the crack remains open during the transient load process.

Consideration of contact between crack surfaces requires a non-linear time stepping procedure, which is out of the scope of this paper.

4.1. Straight crack under impinging waves

This first example corresponds to a straight crack in an infinite plane subjected to waves impinging the crack from different angles as shown in Fig. 1. Only one side of the crack surface has to be discretized. Ten discontinuous quadratic elements are used with the two extreme ones being quarter-point elements. The BE discretization is symmetric with respect to the crack center point with constantly decreasing element length from the crack center towards the tips. The ratio between the center elements and the tip elements is equal to two. Plane strain conditions are assumed.

The analysis of wave diffraction by a crack in an infinite medium is carried out by superposition of two problems. One, the incident field in the uncracked domain, and the other, the cracked domain loaded on the crack faces by tractions equal and opposite to those appearing in the uncracked domain along the crack line. Those tractions, for an orthotropic solid with waves propagating along the material axis of symmetry y can be defined as follows:

P-wave displacements:

$$u_x = 0; \qquad u_y = u_{y0}\exp\left[i\omega\left(\frac{y}{C_p}+t\right)\right]; \qquad C_p = \sqrt{C_{22}/\rho} \tag{39}$$

Stress tensor components:

$$\sigma_x = C_{12}u_{y0}\frac{i\omega}{C_p}\exp\left[i\omega\left(\frac{y}{C_p}\right)\right] := \frac{C_{12}}{C_{22}}\sigma_0\exp\left[i\omega\left(\frac{y}{C_p}\right)\right]$$
$$\sigma_y = C_{22}u_{y0}\frac{i\omega}{C_s}\exp\left[i\omega\left(\frac{y}{C_p}\right)\right] := \sigma_0\exp\left[i\omega\left(\frac{y}{C_p}\right)\right];\ \sigma_{xy} = 0 \tag{40}$$

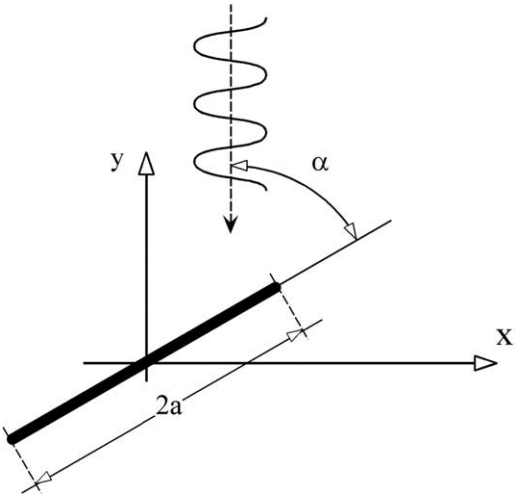

Fig. 1. Straight crack in infinite plane subjected to time-harmonic waves.

Tractions for a surface with outer normal components n_x, n_y:

$$p_x = \frac{C_{12}}{C_{22}}\sigma_0\exp\left[i\omega\left(\frac{y}{C_p}\right)\right]n_x;\ p_y = \sigma_0\exp\left[i\omega\left(\frac{y}{C_p}\right)\right]n_y \tag{41}$$

S-wave:

$$u_x = u_{x0}\exp\left[i\omega\left(\frac{y}{C_s}+t\right)\right]; C_s = \sqrt{C_{66}/\rho};\ u_y = 0 \tag{42}$$

$$\sigma_x = 0;\ \sigma_y = 0$$
$$\sigma_{xy} = C_{66}u_{x0}\frac{i\omega}{C_s}\exp\left[i\omega\left(\frac{y}{C_s}\right)\right] := \tau_0\exp\left[i\omega\left(\frac{y}{C_s}\right)\right] \tag{43}$$

$$p_x = \tau_0\exp\left[i\omega\left(\frac{y}{C_s}\right)\right]n_x;\ p_y = \tau_0\exp\left[i\omega\left(\frac{y}{C_s}\right)\right]n_y \tag{44}$$

Complex-valued notation has been used in Eqs. (39)–(44) to represent domain and boundary variables as usual in time-harmonic dynamic problems. Only the real part of these expressions have a physical meaning.

Since there are not infinite values of the stress in the uncracked plane, the SIF in the original diffraction problem are the same as in the second problem (scattered field). For the sake of simplicity and comparison, numerical results were obtained for an isotropic material with Poisson's ratio $\nu = 0.25$. In such case, $C_{11} = C_{22} = \lambda + 2\mu$ and $C_{66} = \mu$. Fig. 2(a) shows values of the normalized mode-I SIF versus the dimensionless frequency $\omega a/C_p$, were a is the crack half-length and $C_p = [(\lambda + 2\mu)/\rho]^{1/2}$ is the P-wave velocity, for an impinging P-wave. Mode I SIF for an incident S-wave are shown in Fig. 2(b). The present results are compared with those obtained by Chen and Sih [13] using a method including the solution of a system of integral equations. The agreement between both sets of results is very good. Results obtained using the present method for K_{II}, P- and S-waves and different angles of incidence can be found in the work of García-Sánchez [24]. In all cases, these results are in very good agreement with those presented by Chen and Sih [13].

4.2. Parallel cracks in infinite orthotropic plane

The second numerical application corresponds to two parallel cracks separated by a distance h and subjected to time-harmonic waves impinging on the two cracks normal to their surface. The two cracks have the same length and are parallel to the x-axis (Fig. 3). Boundary element discretization for each crack is the same as for the single crack of the previous example. The material is a boron-epoxy (type I) composite with the engineering elastic properties given in Table 1. These properties are taken from Itou and Haliding [29], where the problem is studied using a Fourier transform technique to reduce the boundary conditions to four simultaneous integral equations which are solved expanding the crack opening displacement in a series.

Results for normalized mode-II SIF and two different values of h, when P-waves impinge on the cracks, are shown versus

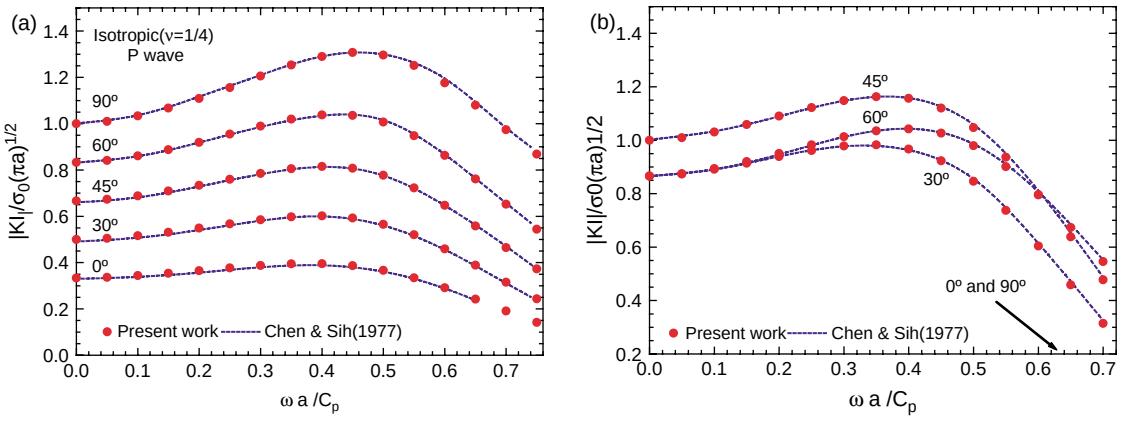

Fig. 2. Mode-I SIF for straight crack in infinite isotropic plane under time-harmonic (a) P-waves; and (b) S-waves.

the dimensionless frequency $\omega a/C_5$ in Fig. 4. The obtained results are compared with those of Itou and Haliding [29]. The agreement between both sets of results is very good. The same agreement exists for mode-I SIF, S-waves, and different orthotropic materials. A more complete parametric analysis of this problem can be seen in the work of García-Sánchez [24].

4.3. Collinear cracks in orthotropic medium

Two equal collinear cracks are assumed to be located along the x-axis of an orthotropic infinite plane as shown in Fig. 5. Time-harmonic waves traveling along the material axis y are interrupted at normal incidence by the line cracks. Once more P- and S-waves are considered. For the sake of comparison with some existing results, two different boron-epoxy composites (type I and type II) with properties as given in Table 1 are considered. The BE discretization consists of 10 symmetrically distributed elements for each crack including quarter-point elements at the crack tips. The size of these elements is the same as in the previous examples.

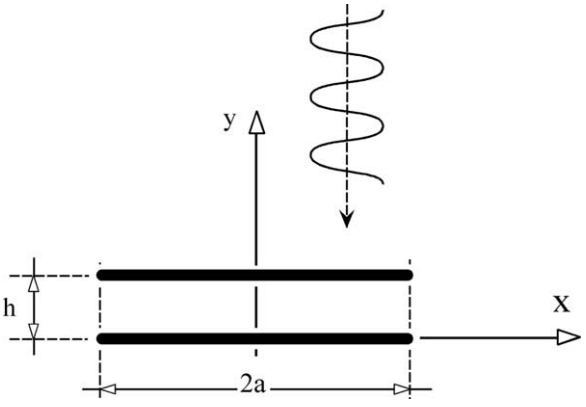

Fig. 3. Parallel cracks in infinite plane under time-harmonic waves.

Table 1
Elastic material properties for boron-epoxy

E_x (GPa)	E_y (GPa)	G_{xy} (GPa)	ν_{xy} (GPa)
Boron-epoxy (type I)			
224.06	12.69	4.43	0.256
Boron-epoxy (type II)			
55.16	170.65	4.83	0.036

Fig. 6 shows some of the obtained results for this problem. Mode-I SIF at the two crack tips are represented versus dimensionless frequency when P-waves impinge on the cracks and the distance between them is half of their length ($h=a/2$). The obtained results are compared with those presented by Itou [28] for the same problem using a semi-analytical approach. The agreement between both sets of results is, once more, very good. A parametric study for different excitation waves and crack distances can be found in the work of García-Sánchez [24]. A very good agreement with Itou's results is observed for all configurations, materials and excitations considered by this author.

4.4. Kinked crack in infinite plane

The crack of this example consists of a straight main crack and a branch initiating from the main crack-tip. There is not restriction on the branch direction. The solid is an infinite plane and the crack is impinged by P- or S-waves traveling perpendicularly to the main crack direction. Two different

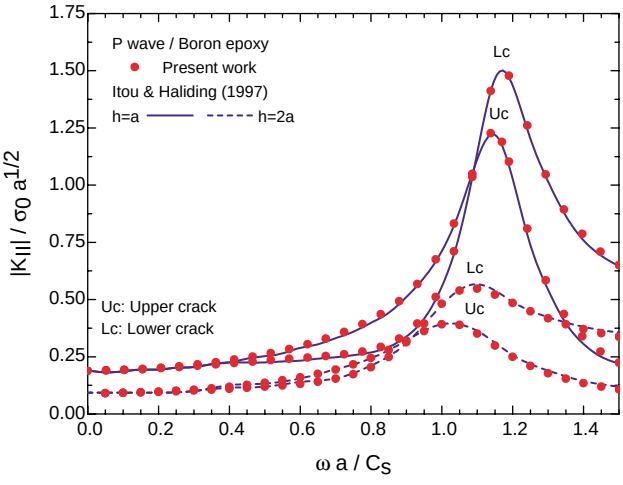

Fig. 4. Mode-II SIF for two parallel cracks in orthotropic plane under time-harmonic P-waves.

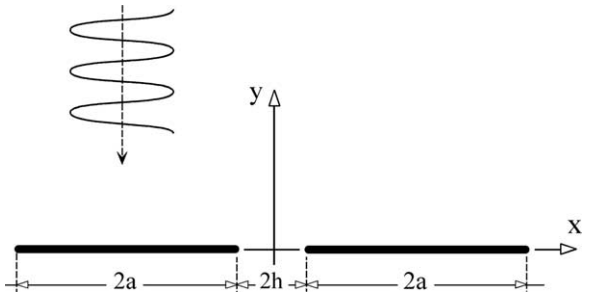

Fig. 5. Collinear cracks in infinite plane under time-harmonic waves.

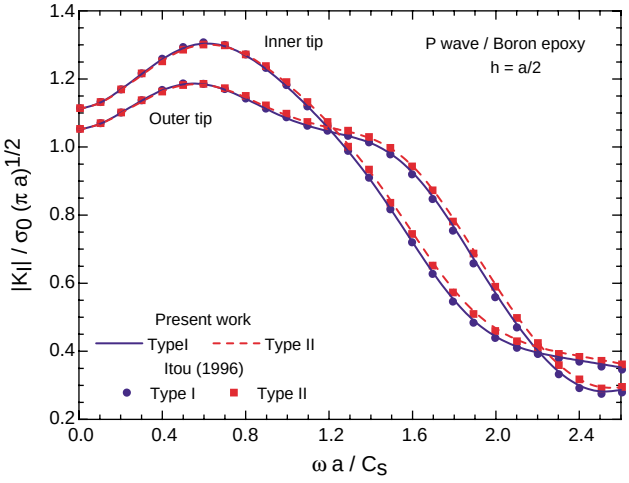

Fig. 6. Mode I SIF for two collinear cracks in orthotropic plane under time-harmonic P-waves.

materials are considered: the type I boron-epoxy defined in Table 1 and an isotropic material with Poisson's ratio $\nu = 0.25$ and shear modulus equal to the G_{12} of the boron-epoxy composite. In the orthotropic material case, the main crack direction coincides with the x-axis and waves propagate along the y-axis (Fig. 7). The BE discretization consists of 12 variable length quadratic elements along the main crack and six elements along the branch. The ratio between the largest

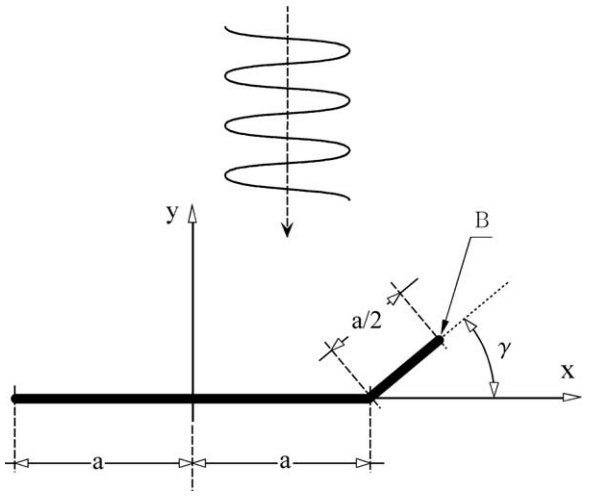

Fig. 7. Kinked crack in infinite plane under time-harmonic waves.

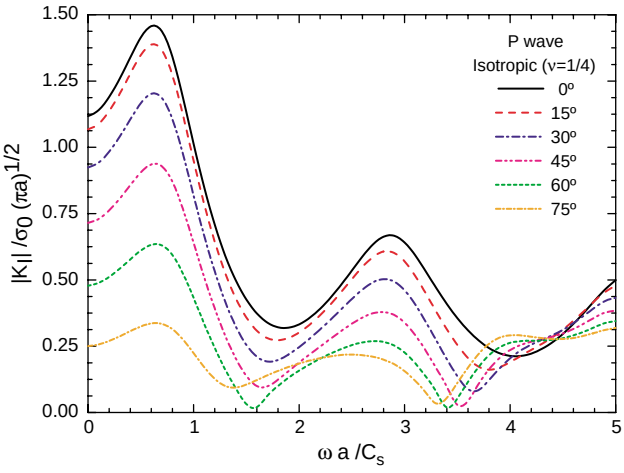

Fig. 8. Mode I SIF at the branch tip for kinked crack in isotropic plane under time-harmonic P-waves.

elements at the center of the main crack and the quarter-point elements at the tips is two.

Values of mode-I SIF at the branch tip when P-waves impinge on the crack are represented versus dimensionless frequency for different crack angles in Figs. 8 and 9. The first figure corresponds to the isotropic material and the second to the boron-epoxy composite. As expected, there is an important effect of the branch angle γ on the K_I SIF. This effect is similar in both cases. Additional results for positive and negative values of γ, P- and S-waves, mode-I and mode-II SIF, can be found in the work of García-Sánchez [24].

4.5. Curved crack in infinite domain

To show the use of the current procedure for curved crack geometries, the problem of a crack with circular arch shape in an unbounded domain is analyzed next. The same two materials of the previous problem are studied. The crack is subjected to incident P- or S-waves traveling along the positive y-axis. Crack geometry and wave propagation direction are

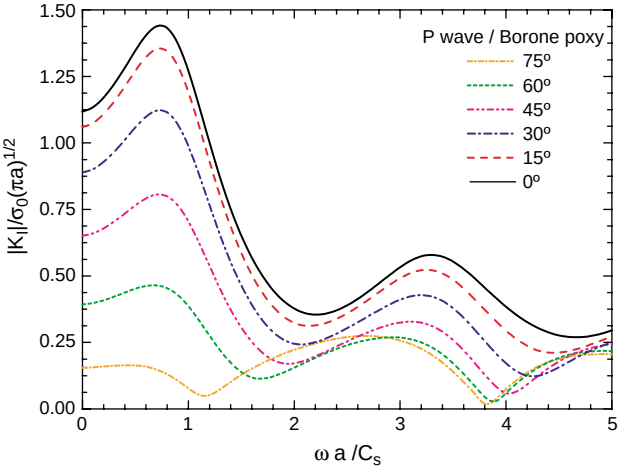

Fig. 9. Mode I SIF at the branch tip for kinked crack in orthotropic plane under time-harmonic P-waves.

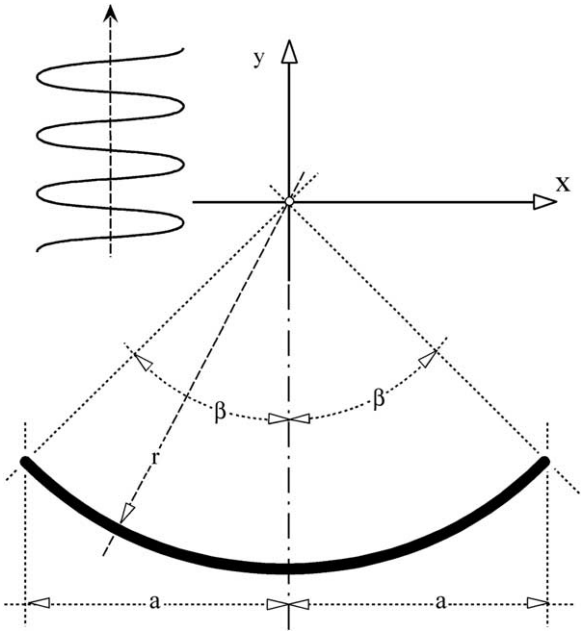

Fig. 10. Circular arch crack in infinite plane under time-harmonic waves.

represented in Fig. 10. Cracks with semi-angles β between 15 and 75° are considered. The BE mesh for any crack angle contains 10 quadratic elements as shown in Fig. 11, where dots indicate extreme points of the elements. Eight of the elements in Fig. 11 are curved quadratic elements whereas the two elements at the crack tips are very small quarter-point straight elements. This type of mesh was shown to yield very accurate results for static anisotropic curved crack problems [23].

Computed mode-I SIF for incident P-waves and different crack semi-angles are represented versus frequency in Fig. 12 for the isotropic material and Fig. 13 for the boron-epoxy composite. It can be seen from these results that the influence of the material anisotropy is not very important in this case and that the frequency variation is somehow similar to that of the kinked crack with the same angle (Figs. 8 and 9). Nevertheless, significant differences between isotropic and anisotropic material appear when S-waves impinge on the crack. This fact can be observed in Figs. 14 (isotropic) and 15 (boron-epoxy) where values of mode-I SIF for this kind of waves are represented versus frequency. It should be noticed that the isotropic material has properties in any direction similar to those of the orthotropic material along the wave propagation direction. In the S-wave case, displacements associated to the

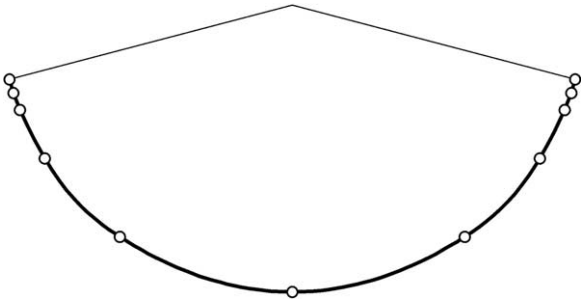

Fig. 11. BE mesh for circular arch crack.

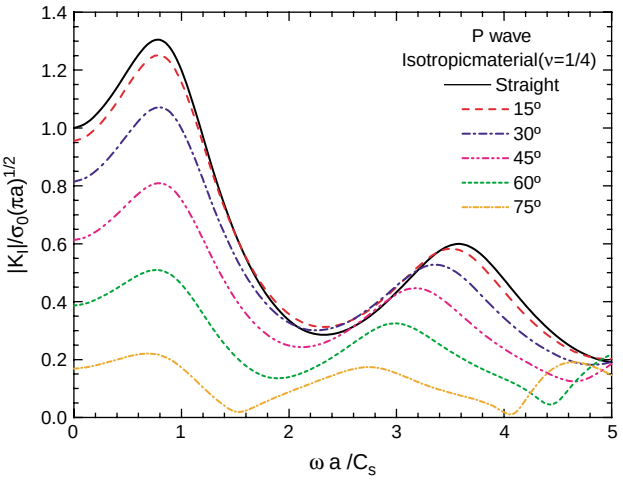

Fig. 12. Mode I SIF for circular crack in isotropic plane under time-harmonic P-waves.

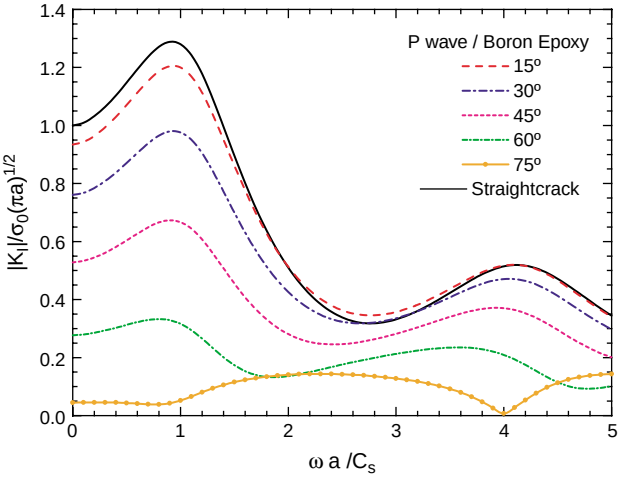

Fig. 13. Mode I SIF for circular crack in orthotropic plane under time-harmonic P-waves.

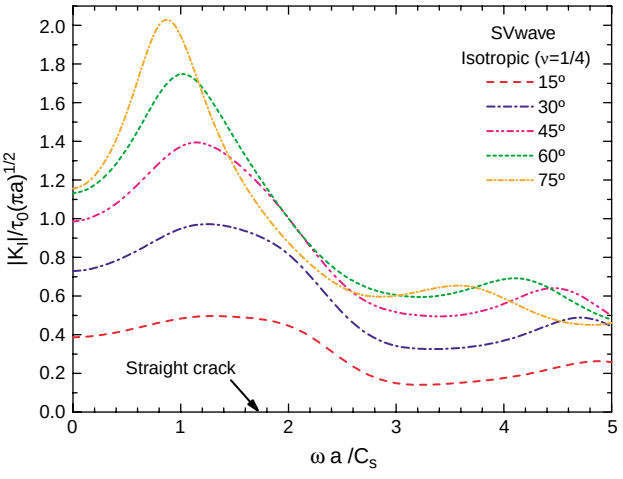

Fig. 14. Mode I SIF for circular crack in isotropic plane under time-harmonic S-waves.

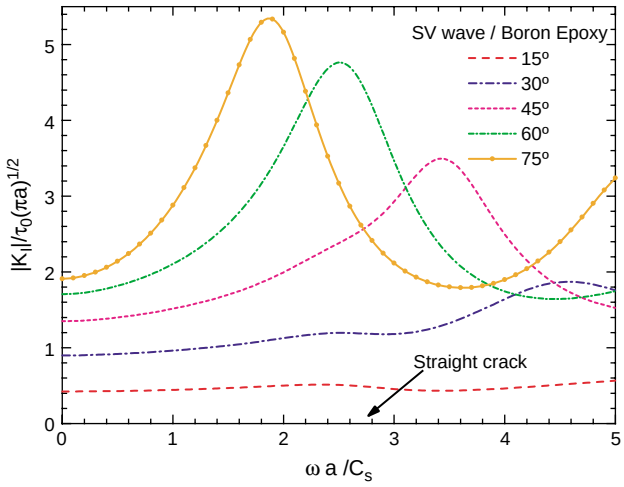

Fig. 15. Mode I SIF for circular crack in orthotropic plane under time-harmonic S-waves.

impinging waves are perpendicular to that direction. Additional results for mode-II SIF and for different orthotropic material properties may be found in Ref. [24].

4.6. Central crack in rectangular plate

The following application has been taken from Chirino and Domínguez [14], and shows how the mixed formulation proposed can be used for bounded domain problems. Fig. 16

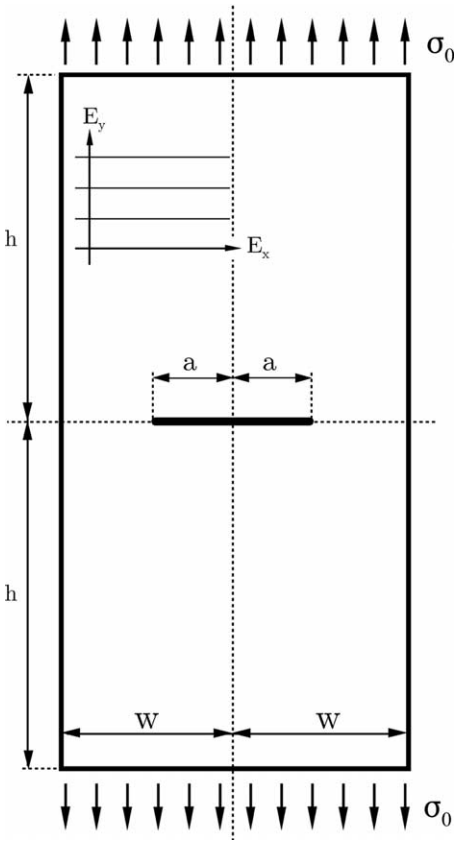

Fig. 16. Rectangular plate with central crack.

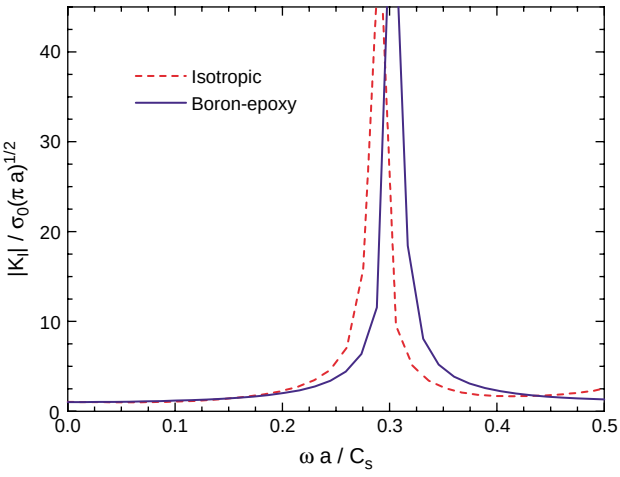

Fig. 17. Normalized mode-I SIF for central crack in rectangular plate.

shows the geometry and boundary conditions of a rectangular cracked plate. A uniform time-harmonic traction is applied at two opposite sides of the plate. The BE discretization consist of 10 discontinuous quadratic elements for the crack with the two extreme ones being quarter-point and 36 equal quadratic elements at the external boundary. The size of the crack elements varies with a constant rate from the center of the crack towards the end, the ratio between the length of the two central elements and the two tip elements being equal to two. The traction boundary integral equation is applied for the nodes along the crack and the displacement boundary integral equation for the nodes on the external boundary. The variables of the problem are the crack opening displacements and the external boundary displacements and tractions. Two different materials are considered. One is the same isotropic material as considered in Ref. [14]. The second material is the same type I boron-epoxy composite considered in previous applications of the present paper.

The normalized mode-I SIF for the two materials is shown versus dimensionless frequency of the excitation in Fig. 17. Results for the isotropic case coincide with those of Chirino and Domínguez [14] using the classical formulation and symmetry conditions. The effect of material anisotropy can be appreciated in Fig. 17, in particular the change in position of the resonance peak.

5. Conclusions

A mixed BEM formulation for 2D time-harmonic dynamic fracture problems in solids of general anisotropy has been proposed. This work is the dynamic counterpart of a previous static BEM formulation [23]. The time-harmonic Green's functions derived by Wang and Achenbach [53] are split into singular static plus regular frequency dependent parts. In this way, the singular and hypersingular integrals that arise from the singular part of the fundamental solution are regularized as in the elastostatic case [23] by means of a simple change of variable. Subsequently, the regular part is added-up in order to solve the dynamic problem. The regular (frequency dependent)

part is given in terms of line integrals over a unit circle that are numerically evaluated.

The accuracy and robustness of the present BEM approach has been demonstrated by comparison of the obtained results with some published solutions. Several other examples including kinked and curved crack geometries have been presented for the first time.

Acknowledgements

We are thankful to the anonymous reviewers for their useful suggestions. This work was supported by the Ministerio de Ciencia y Tecnología of Spain (DPI2004-08147-C02-02). The financial support is gratefully acknowledged.

References

[1] Ahmad S, Leyte F, Rajapakse RKND. BEM analysis of two-dimensional elastodynamic problems of anisotropic solids. ASCE J Eng Mech 2001; 127:149–56.
[2] Alburquerque EL, Sollero P, Fedelinski P. Free vibration analysis of anisotropic material structures using the boundary element method. Eng Anal Bound Elem 2003;27:977–85.
[3] Alburquerque EL, Sollero P, Aliabadi MH. The boundary element method applied to time dependent problems in anisotropic materials. Int J Solids Struct 2002;39:1405–22.
[4] Alburquerque EL, Sollero P, Fedelinski P. Dual reciprocity boundary element method in Laplace domain applied to anisotropic dynamic problems. Comput Struct 2003;81:1703–13.
[5] Alburquerque EL, Sollero P, Aliabadi MH. Dual boundary element method for anisotropic dynamic fracture mechanics. Int J Numer Methods Eng 2004;59:1187–205.
[6] Aliabadi MH. Boundary element formulations in fracture mechanics. ASME Appl Mech Rev 1997;50:83–96.
[7] Ang WT, Park YS. Hypersinglar integral equations for arbitrarily located planar craks in an anisotropic elastic bimaterial. Eng Anal Bound Elem 1997;20:135–43.
[8] Ariza MP, Domínguez J. Boundary element formulation for 3-D transversely isotropic cracked bodies. Int J Numer Methods Eng 2004; 60:719–53.
[9] Ariza MP, Domínguez J. BE analysis of 3-D cracks in transversely isotropic solids. Comput Methods Appl Mech Eng 2004;193:765–79.
[10] Beskos DE. Boundary element methods in dynamic analysis. ASME Appl Mech Rev 1987;40:1–23.
[11] Beskos DE. Boundary element methods in dynamic analysis: part II (1986–1996). ASME Appl Mech Rev 1997;50:149–97.
[12] Blandford GE, Ingraffea AR, Liggett JA. Two-dimensional stress intensity factor computations using the boundary element method. Int J Numer Methods Eng 1981;17:387–404.
[13] Chen EP, Sih GC. Scattering waves about stationary and moving cracks. In: Sih GC, editor. Mechanics of fracture: elastodynamic crack problems. Leyden: Noordhoff; 1977. p. 119–212.
[14] Chirino F, Domínguez J. Dynamic analysis of cracks using boundary element method. Eng Fract Mech 1989;34:1051–61.
[15] Cruse TA, Swedlow JL. Interactive program for analysis and design problems in advanced composites technology. Report AFML-TR-71-268. Carnegie-Mellon University; 1971.
[16] Cruse TA, Wilson RB. Boundary integral equation method for elastic fracture mechanics analisys, AFOSR-TR-780355. Pratt and Wihtney Aircraft Group; 1977.
[17] Denda M, Wang CY, Yong YK. 2-D time harmonic BEM for solids of general anisotropy with application to eigenvalue problems. J Sound Vib 2003;261:247–76.
[18] Dineva P, Rangelov T, Gross D. BIEM for 2D steady-state problems in cracked anisotropic materials. Eng Anal Bound Elem 2005;29:689–98.
[19] Doblaré M, Espiga F, Gracia L, Alcantud M. Study of crack propagation in orthotropic materials by using the boundary element method. Eng Fract Mech 1990;37:935–67.
[20] Domínguez J. Boundary elements in dynamics. Southampton/London: Comput. Mech. Publ./Elsevier; 1993.
[21] Dravinski M, Niu Y. Three-dimensional time-harmonic Green's functions for a triclinic full-space using a symbolic computation system. Int J Numer Methods Eng 2002;53:455–72.
[22] Eshelby JD, Read WT, Shockley W. Anisotropic with applications to dislocation theory. Acta Metall 1953;1:251–9.
[23] García F, Sáez A, Domínguez J. Traction boundary elements for cracks in anisotropic solids. Eng Anal Bound Elem 2004;28:667–76.
[24] García-Sánchez F. Numerical study of fracture problems in anisotropic elastic and piezoelectric solids (in Spanish). PhD Thesis. University of Sevilla, Spain; 2004.
[25] Hirose S, Zhang Ch, Wang C-Y. A comparative study on two time domain BEM/BIEM for transient dynamic crack análisis of anisotropic solids. In: Yao Z, Aliabadi MH, editors. Proceedings of Beteq third international conference. Beijing: Tsinghua University Press/Springer; 2002.
[26] Hong H-K, Chen JT. Derivations of integral equations of elasticity. J Eng Mech 1988;114:1028–44.
[27] Ioakimidis NI. A new singular integral equation for the classical crack problem in plane and antiplane elaticity. Int J Fract 1983;21:115–22.
[28] Itou S. Dynamic stress intensity factors of two collinear cracks in orthotropic medium subjected to time-harmonic disturbance. Theor Appl Fract Mech 1996;25:155–66.
[29] Itou S, Haliding H. Dynamic stress intensity factors around two parallel cracks in an infinite orthotropic plane subjected to incident harmonic stress waves. Int J Solids Struct 1997;34:1145–65.
[30] Kobayashi S, Nishimura N, Kishima T. A BIE analysis of wave propagation in anisotropic media. In: Proceedings of boundary elements VIII. Berlin: Springer; 1986. p. 425–4.
[31] Kögl M, Gaul L. A 3-D boundary element method for dynamic analysis of anisotropic elastic solids. Comput Model Eng Sci 2000;1:27–43.
[32] Martínez J, Domínguez J. On the use of quarter-point boundary elements for stress intensity factor computation. Int J Numer Methods Eng 1984; 20:1941–50.
[33] Niu Y, Dravinski M. Three-dimensional BEM for scattering of elastic waves in general anisotropic media. Int J Numer Methods Eng 2003;58: 978–98.
[34] Pan YC, Chou TW. Point force solution for an infinite transversely isotropic solid. ASME J Appl Mech 1976;43:608–12.
[35] Pan E, Amadei B. Fracture mechanics analysis of cracked 2-D anisotropic media with a new formulation of the boundary element method. Int J Fract 1996;77:161–74.
[36] Pan E. A general boundary element analysis of 2-D linear elastic fracture mechanics. Int J Fract 1997;88:41–59.
[37] Pan E, Chen C-S, Amadei B. A BEM formulation for anisotropic half-plane problems. Eng Anal Bound Elem 1997;20:185–95.
[38] Pan E, Yuan FG. Boundary element analysis of three-dimensional cracks in anisotropic solids. Int J Numer Methods Eng 2000;48:211–37.
[39] Sáez A, Gallego R, Domínguez J. Hypersingular quarter-point boundary elements for crack problems. Int J Numer Methods Eng 1995;38: 1681–701.
[40] Sáez A, Ariza MP, Domínguez J. Three-dimensional fracture analysis in transversely isotropic solids. Eng Anal Bound Elem 1997;20:287–98.
[41] Sáez A, Domínguez J. BEM analysis of wave scattering in transversely isotropic solids. Int J Numer Methods Eng 1999;44:1283–300.
[42] Sáez A, Domínguez J. Dynamic crack problems in three-dimensional transversely isotropic solids. Eng Anal Bound Elem 2001;25:203–10.
[43] Sih GC, Paris PC, Irwin GR. On cracks in rectilinearly anisotropic bodies. Int J Fract Mech 1965;1:189–203.
[44] Smith RNL, Mason JC. A boundary element method for curved crack problems in two dimensions. In: Brebbia CA, editor.

Boundary element methods in engineering. Proceedings of fourth international conference on boundary elements. Berlin: Springer; 1982. p. 472–84.

[45] Snyder MD, Cruse TA. Boundary integral equation analysis of craked anisotropic plates. Int J Fract 1975;11:315–28.

[46] Sollero P, Aliabadi MH. Fracture mechanics analysis of anisotropic plates by the boundary elment method. Int J Fract 1993;64:269–84.

[47] Sollero P, Aliabadi MH, Rooke DP. Anisotropic analysis of craks emanating from circular holes in composite laminates using the boundary element method. Eng Fract Mech 1994;49:213–24.

[48] Sollero P, Aliabadi MH. Anisotropic analysis of cracks in composite laminates using the dual boundary element method. Comput Struct 1995; 31:22–233.

[49] Tan CL, Gao YL. Boundary element analysis of plane anisotropic bodies with stress concentration and cracks. Comput Struct 1992;20:17–28.

[50] Tanaka M, Sladek V, Sladek J. Regularization techniques applied toboundary element methods. ASME Appl Mech Rev 1994;47: 457–99.

[51] Tonon F, Pan E, Amadei B. Green's functions and boundary element method formulation for 3D anisotropic media. Comput Struct 2002;39: 2235–55.

[53] Wang C-Y, Achenbach JD. Elastodynamic fundamental solutions for anisotropic solids. Geophys J Int 1994;118:384–92.

[54] Wang C-Y, Achenbach JD. 3-D time-harmonic elastodynamic Green's functions for anisotropic solids. Proc R Soc Lond 1995;A449:441–58.

[55] Wang C-Y, Achenbach JD, Hirose S. Two-dimensional time domain BEM for scattering of elastic waves in solids of general anisotropy. Int J Solids Struct 1996;33:3843–64.

[56] Zhang Ch. A 2-D time-domain BIEM for dynamic analysis of cracked orthotropic solids. Comput Model Eng Sci 2002;3:381–98.